Published in final edited form as:
Chem Biol. 2013 August 22; 20(8): 991–1001. doi:10.1016/j.chembiol.2013.06.011.

Peroxiredoxin-1 from the human hookworm *Ancylostoma ceylanicum* forms a stable oxidized decamer and is covalently inhibited by conoidin A

Jennifer B. Nguyen[1], **Christopher D. Pool**[2], **Christina Y.B. Wong**[2], **Rebecca S. Treger**[2], **David L. Williams**[3], **Michael Cappello**[2], **Wendy A. Lea**[4], **Anton Simeonov**[4], **Jon J. Vermeire**[2], and **Yorgo Modis**[1,*]

[1]Department of Molecular Biophysics and Biochemistry, Yale University, New Haven, CT 06520

[2]Program in International Child Health and Department of Pediatrics, Yale University School of Medicine, Child Health Research Center 464 Congress Avenue, New Haven, CT 06520-8081

[3]Department of Immunology-Microbiology, Rush University Medical Center, Chicago, IL 60612

[4]NIH Chemical Genomics Center, National Human Genome Research Institute, National Institutes of Health, Bethesda, MD 20892-3370

Summary

Hookworms are parasitic nematodes that have a devastating impact on global health, particularly in developing countries. We report a biochemical and structural analysis of a peroxiredoxin from the hookworm *Ancylostoma ceylanicum*, AcePrx-1. Peroxiredoxins provide antioxidant protection and act as signaling molecules and chaperones. AcePrx-1 is expressed in adult hookworms and can be inactivated by 2,3-bis(bromomethyl)quinoxaline-1,4-dioxide (conoidin A). Conoidin A inactivates AcePrx-1 by alkylating or crosslinking the catalytic cysteines, while maintaining the enzyme in the "locally unfolded" conformation. Irreversible oxidation of the resolving cysteine may contribute additional inhibitory activity. A crystal structure of oxidized AcePrx-1 reveals a disulfide-linked decamer. A helix macrodipole near the active site increases the reactivity of the catalytic cysteines to conoidin A. This work demonstrates the promise of conoidin compounds as probes to evaluate peroxiredoxins as drug targets in human parasites.

Introduction

Hookworms are intestinal nematodes that rank as top agents of global morbidity (Bungiro and Cappello, 2011; Hotez, et al., 2004). Human hookworm disease is caused by three

*To whom correspondence should be addressed: 266 Whitney Ave, Bass 430, New Haven, CT 06520, USA, Tel.: (203) 432-4330; Fax: (203) 436-4369; yorgo.modis@yale.edu.

Accession Numbers

The nucleotide and translated amino acid sequences for AcePrx-1 have been deposited in GenBank with accession code JX124321. The atomic coordinates and experimental structure factors for AcePrx-1 have been deposited in the Protein Data Bank with accession codes 4FH8 and 4KW6.

Supplemental Information

Additional supplemental information may be found in the online version of this article.

hookworm species, *Necator americanus*, *Ancylostoma duodenale* and *Ancylostoma ceylanicum*. Nearly one billion people suffer hookworm infection, which is characterized by iron deficiency anemia, malnutrition and suppression of host cellular immune responses (Geiger, et al., 2004; Loukas, et al., 2005; Maizels and Yazdanbakhsh, 2003). Hookworms and other soil transmitted nematode infections are most prevalent in children in developing countries (Awasthi, et al., 2003), although infection occurs in all age groups and may exacerbate other common infectious diseases, including tuberculosis, malaria, and human immunodeficiency virus (Bundy, et al., 2000; Onyemelukwe and Musa, 2001; Roussilhon, et al., 2010). Although community based deworming programs may have short-term benefit, rapid reinfection rates and declining efficacy of commonly used anthelminthics raise doubts about the long-term value of chemotherapy as an effective means of disease control (Albonico, et al., 2004; Humphries, et al., 2012; Keiser and Utzinger, 2008).

As blood feeding parasites, hookworms must handle the challenges of storage, sequestration and detoxification of heme groups. The components of the heme group are capable of producing toxic reactive oxygen species (ROS), such as free hydroxyl radicals and singlet oxygen molecules (Toh, et al., 2010). ROS are also released by host immune effector cells such as macrophages, eosinophils, and neutrophils in their response to hookworm infection (Donnelly, et al., 2010; Hofmann, et al., 2002). Hookworms express at least two peroxiredoxins, a family of peroxidases important for protection against ROS, protein folding (Tavender, et al., 2010; Zito, et al., 2010) and intracellular signaling (reviewed in Hall, et al., 2009; Winterbourn, 2008). Certain peroxiredoxins, including PrxI from the human trematode *Schistosoma mansoni*, also function as redox-regulated ATP-independent chaperones (Jang, et al., 2004; Saccoccia, et al., 2012). Peroxiredoxins are widely conserved across eukaryotes (Figure 1). The active site of the “typical” class of peroxiredoxins is formed at the intersubunit interface of homodimers, which can assemble into rings of ten or twelve subunits (Cao, et al., 2011; Nelson, et al., 2011; Schroder, et al., 2000). A catalytic peroxidatic cysteine residue reduces peroxide and other ROS, resulting in hyperoxidation to sulfenic (-SOH), sulfinic ($-SO_2H$), or sulfonic acid ($-SO_3H$) forms of the cysteine. The sulfenic acid form reacts with a second so-called resolving catalytic cysteine residue across the dimer interface to form an intermolecular disulfide bond. Oxidation to sulfinic acid can be repaired by sulfiredoxin, while the sulfonic acid form is considered irreversible (Cao, et al., 2011; Nelson, et al., 2011; Schroder, et al., 2000).

In humans, changes in peroxiredoxin expression levels are associated with cancer, cardiovascular dysfunction and neurodegeneration (Park, et al., 2000). Hence, there is significant clinical interest in human peroxiredoxin inhibitors. A cell permeable organic compound, 2,3-bis(bromomethyl)quinoxaline-1,4-dioxide (conoidin A), has been shown to inhibit the hyperoxidation activity of peroxiredoxin II from the apicomplexan parasite *Toxoplasma gondii* (TgPrxII), as well as human peroxiredoxins I and II (Haraldsen, et al., 2009). Conoidin A inhibits TgPrxII with an IC_{50} of 23 μM by binding covalently to the peroxidatic cysteine (Liu, et al., 2010). More relevant to the present study, conoidin A treatment of *A. ceylanicum* eggs purified from the feces of infected hamsters as well as eggs from field isolates of human hookworms resulted in a significant inhibition of egg hatching, revealing the nematicidal activity of conoidin A (Treger, et al., 2013).

Here, we show that peroxiredoxin-1 from *A. ceylanicum* (AcePrx-1) is expressed in adult worms and inactivated by conoidin A. Biophysical analyses and a crystal structure of oxidized AcePrx-1 show that it forms a stable decamer, similar to human peroxiredoxin IV (Cao, et al., 2011). The active site architecture increases the reactivity of the two catalytic cysteine residues to conoidin A. Conoidin A inhibits AcePrx-1 by alkylating cysteines, crosslinking the catalytic cysteines, or possibly oxidizing one or both of the catalytic cysteines to an irreversible oxidation state, while maintaining the enzyme in the so-called

locally unfolded (LU) conformation. This work demonstrates the potential applicability of conoidin compounds as chemical probes to evaluate AcePrx-1 and related enzymes as possible drug targets in *A. ceylanicum* and other human parasites.

Results

AcePrx-1 is highly expressed and partially excreted/secreted by adult A. ceylanicum

Real-time PCR analysis of cDNA populations created from egg, larval and adult *A. ceylanicum* showed that the AcePrx-1 mRNA transcript is present in much higher abundance in adult (female or male) worms compared to egg (E) and (L1 or L3) larval stages (37- and 24-fold higher, respectively, Figure 2A). Western blot analysis of egg, larval and adult stages of *A. ceylanicum* verified this finding, revealing that AcePrx-1 is produced by adult worms and is present in extracts (HEX) and excretory/secretory (ES) products (Figure 2A). Protein levels in egg and larval stages were below detection level by immunoblotting.

AcePrx-1 is an active peroxidase and is inhibited by conoidin A

The specific activity of recombinant AcePrx-1 peroxide metabolism was determined to be 1.640 μmol min^{-1} mg^{-1} compared to 1.182 μmol min^{-1} mg^{-1} for human PrxII (hPrxII) and 1.616 μmol min^{-1} mg^{-1} for human Prx-IV (hPrxIV). As expected, a triple cysteine mutant (C49A/C73A/C170A) of AcePrx-1, which lacked the peroxidatic and resolving cysteine residues, exhibited no activity (Figure 2B). Conoidin A or its mono-brominated analog, 2-(bromomethyl)-3-quinoxaline-1,4-dioxide (conoidin B), inhibited the activity of wild type AcePrx-1, hPrxII, and hPrxIV in a dose-dependent manner up to the solubility limit of the compounds with IC_{50} values of 374, 358, and 262 μM, respectively, for conoidin A (Figure 2C-D). At inhibitor concentrations above those tested in Figure 2D (120 μM), the compounds precipitated, interfering with the assay. Conoidin A and conoidin B inhibition profiles were similar for AcePrx-1, hPrxII and hPrxIV, indicating that these compounds do not have specificity for the hookworm protein.

Conoidin A hyperoxidizes the catalytic cysteines and reacts covalently with all three AcePrx-1 cysteines

To determine whether AcePrx-1 reacts covalently with conoidin A and whether the reaction occurs via the catalytic cysteines, we analyzed wild type and mutant AcePrx-1 proteins by SDS-PAGE and mass spectrometry after treatment with conoidin A. As expected for a 2-Cys peroxiredoxin, AcePrx-1 was mostly dimeric in non-reducing SDS-PAGE and monomeric under reducing conditions (Figure 3A-B). Three distinct bands could be distinguished under non-reducing conditions, presumably corresponding to 0, 1, and 2 disulfide bonds within the dimer, respectively. Mutations at either or both of the active site cysteine residues (Cys49, Cys170) rendered the protein predominantly monomeric (Figure 3A). A C-terminal truncation at residue 171 (Δ171) did not affect this dimerization pattern. These data confirm that AcePrx-1 forms disulfide-linked dimers via its active site cysteine residues.

AcePrx-1 incubated for at least 30 min with a three-fold molar excess of conoidin A or conoidin B produced dimer bands in SDS-PAGE (one faint dimer band for conoidin B and two strong bands for conoidin A), in addition to the monomer band (Figure 3B). Mutation of Cys49, Cys170, or both resulted in a marked reduction in the proportion of dimeric species in the presence of conoidin under reducing conditions (Figure 3D). Low levels of several discrete species of higher order oligomers were also observed in the presence of conoidin A/B, ranging up to approximately a decamer, even under reducing conditions (Figure 3D). Dose-dependent formation of high molecular-weight complexes upon reaction with conoidin

A has been observed previously with hPrxII (Haraldsen, et al., 2009). Small quantities of crosslinked species in the C49A/C73A/C170A mutant (Figure 3D) may be attributable to nonspecific covalent (or non-covalent SDS-resistant) crosslinks by conoidin A to non-cysteine residues. Together, these data suggest that conoidin A covalently crosslinks AcePrx-1 mainly via the active site cysteines to form AcePrx-1 dimers.

To definitively identify the crosslinking sites within the dimers, wild type and mutant AcePrx-1 proteins were subjected to liquid chromatography and electrospray ionization mass spectrometry (LC-ESI-MS) with and without pretreatment with conoidin A or conoidin B. Untreated wild type AcePrx-1 produced two peaks, corresponding to AcePrx-1 monomers and disulfide-linked dimers, with masses of 22,960.0 and 45,920.0 Da, respectively (Figure 4A and Table S1). Additional peaks of 23,004.5 and 23,049.0 Da for the monomer and 46,009.0 and 46,179.0 for the dimer represent different ionization states of the protein. Thus, LC-ESI-MS analysis confirms that wild type AcePrx-1 forms covalently-linked dimers.

A 30-min incubation with conoidin A resulted in a 187-188 Da quinoxaline dioxide (QDO) adduct on the monomer (Figure 4A and Table S1; the 1-Da spread in the mass shift is likely due to slightly different charge states upon ionization). The major product was a 46,294.5 Da species, corresponding to two QDO adducts bridging the peroxidatic and resolving cysteines within a dimer. Displacement of a single bromine on conoidin A would have resulted in a 268 Da adduct, which was not observed under these conditions, suggesting that nucleophilic displacement of the first bromine promotes displacement of the second. Peaks corresponding to unmodified protein were not detected in the conoidin A-treated samples. We conclude that the primary mechanism of AcePrx-1 inactivation by conoidin A is covalent crosslinking of the dimer.

Conoidin B reacted to wild type AcePrx-1 to produce a 189-Da adduct in LC-ESI-MS, although the alkylation reaction was less efficient. Even after incubation for 1 h, most of the protein was unmodified. Data collected after an extended incubation period of 6 h produced noisier data and revealed multiple species in solution. The major peak, with a mass shift of 377.5, corresponded to alkylation at two sites by QDO adducts. A mass shift of 221.0 Da suggests (hyper)oxidation of one or both of the catalytic cysteines. Two additional minor peaks were observed, corresponding to a single QDO adduct and what was presumably a triple (528 Da) substitution containing a mixture of QDO, quinoxaline monoxide (QMO), and/or quinoxaline (Qx) adducts. We note that we could not distinguish between SO_2H and 2•SOH. Although unexpected, the cysteine hyperoxidation is consistent with the propensity of quinoxaline N-oxide compounds to undergo successive one-electron reduction to mono-N-oxide or deoxygenated quinoxaline metabolites (reviewed in González, et al., 2007). This reaction is likely facilitated by oxidation of the highly reactive catalytic cysteine thiols. While sulfenylation of Cys49 is part of the catalytic mechanism, the observed oxidation of Cys170 should inhibit disulfide bond formation with Cys49 and hence inactivate the enzyme. Hyperoxidation of the resolving cysteine (Cys170) therefore provides a possible alternative mechanism to crosslinking for the inactivation of AcePrx-1 by conoidin A. However, hyperoxidized species were only observed after several hours of incubation with conoidin, and these species were less abundant than crosslinked species, so hyperoxidation is not expected to be the primary mechanism of inhibition.

LC-ESI-MS data obtained from C-terminal tail deletion mutants (Δ171 and C49A/C73A/Δ171) and the double- and triple-cysteine mutants (C49A/C170A and C49A/C73A/C170A) produced spectra with low noise levels (Figure 4B-C, Figure S1), even after a 24-h incubation with conoidin A or B. Notably, while conoidin B treatment of the Δ171 sample resulted in a slight shift towards the monomeric form, conoidin A treatment resulted in a

shift towards the dimer form with the masses of the two predominant species shifted by 373 Da and 186 Da, respectively. These mass shifts are consistent with crosslinks by one or two quinoxaline dioxide (QDO) adducts. Since no changes in mass were observed in the C49A/C170A double mutant (Figure 4C) and C49A/C73A/C170A triple mutant (Figure S1), we conclude that the specific sites of modification are the peroxidatic and resolving cysteine residues. A 223 Da adduct was observed in the C49A/C73A/Δ171 mutant treated with conoidin A, corresponding to specific alkylation and hyperoxidation to sulfinic acid of Cys170 (Figure S1B). A summary of the LC-ESI-MS data is provided in Table S1. Together, the mass spectrometry data suggest that the primary mechanism of AcePrx-1 inactivation by conoidin A is covalent crosslinking of the active site cysteines across the dimer interface, with hyperoxidation of the resolving cysteine as a possible secondary mechanism.

Overall structure of AcePrx-1

The crystal structure of AcePrx-1 determined in the absence of reducing agent at 2.1 Å resolution (see Table 1 for crystallographic statistics) reveals a decamer assembled from five AcePrx-1 dimers. The decamer has a ring-shaped $(\alpha_2)_5$ architecture with 52-point group symmetry (Figure 5). Size-exclusion chromatography and multi-angle light scattering data show that AcePrx-1 is also a decamer in solution (Figure S2). The overall structure of AcePrx-1 is similar to that of typical 2-Cys peroxiredoxins. The most similar structure in the Protein Data Bank is human peroxiredoxin IV (PrxIV; PDB code 3TJB) (Cao, et al., 2011). AcePrx-1 closely resembles PrxIV, with a root-mean-square deviation (RMSD) of 0.60 Å for an all-atom superposition of the two proteins. Like AcePrx-1, PrxIV also forms a stable decamer in its oxidized state (Tavender, et al., 2008). In contrast, other typical 2-Cys peroxiredoxins dissociate into dimers in the oxidized state, as demonstrated for example for AhpC from *Salmonella typhimurium* (Wood, et al., 2002).

Each monomer within the AcePrx-1 decamer has the same overall fold as other oxidized typical 2-Cys peroxiredoxins, with five α-helices surrounding a central four-stranded β-sheet and a disordered C-terminal tail (Figure 5C). Residues 171-196 are disordered in each of the ten subunits. The RMSDs of the atom positions between pairs of monomers within the decamer range from 0.22 Å to 0.36 Å.

AcePrx-1 monomers within the decamer form two types of intermolecular interfaces. The more extensive interface is essentially identical to the head-to-tail dimer interface that is conserved in all peroxiredoxins, many of which are obligate dimers. Most of the contacts in this interface are formed by residues 137-163. The β7 strands of the two subunits across the interface form antiparallel β-sheet contacts, thereby merging the central β-sheets of each subunit into an eight-stranded sheet spanning the entire dimer (Figure 5C). The total surface area buried in the dimer interface is 1936 $Å^2$. As in other oxidized peroxiredoxins, the region surrounding the peroxidatic cysteine, Cys49, is in the so-called “locally unfolded” conformation (Hall, et al., 2009). The loop bearing the resolving cysteine, Cys170, is in close proximity to Cys49 and has a high degree of thermal motion as evidenced by the high temperature factors of the corresponding atoms (Figure S3). A notable feature of the dimer interface is a large cavity between strands β7 and helices α5 of the two subunits. The cavity, which is also present in PrxIV, contains 10-12 structured water molecules.

The second intermolecular interface within the AcePrx-1 decamer, between the obligate dimers, involves helix α3 and buries a substantial surface area of 1276 $Å^2$, consistent with our observation that AcePrx-1 is a decamer in solution. The interface is stabilized by a hydrogen bond between the side chain of His107 and a backbone oxygen atom from the adjacent subunit, and by π-stacking interactions between His107 side chains from adjacent subunits. By stabilizing this second intermolecular interface, these interactions may

contribute to the stability of the AcePrx-1 decamer in solution. In support of this hypothesis, His107 is conserved in PrxIV but not in human PrxII (Figure 1), which disassembles into dimers in the oxidized disulfide-bonded form. AcePrx-1 contains an N-terminal histidine tag, and we note that a similar tag was reported to stabilize the oligomeric form of another oxidized peroxiredoxin (Cao, et al., 2007). However, AcePrx-1 containing a C-terminal histidine tag also formed stable decamers in dilute solutions, suggesting that the N-terminal histidine tag alone does not confer stability to the decamer (Figure S2C and D).

Active site structure of AcePrx-1

The active site of peroxiredoxins undergoes a conformational rearrangement during catalysis, cycling between a “fully folded” state during the peroxidation step and a “locally unfolded” state upon resolution of the Cys49 sulfenic acid by Cys170 to form a disulfide (Hall, et al., 2009). In the fully folded form the peroxidatic cysteine thiol is bound in a conserved pocket, whereas in the locally unfolded state the end of helix α2, bearing the peroxidatic cysteine, and helix α6, bearing the resolving cysteine, unwind to bring the two cysteines in position for disulfide bonding. In the structure of AcePrx-1, the enzyme is in the locally unfolded form (Figure 6), as was expected based on the oxidizing environment of the protein during purification and crystallization. A disulfide bond is clearly visible in the electron density for two of the ten subunits (Figure 6A). In the remaining subunits, electron density is lacking for the disulfide bond (Figure 6B), as was also the case for PrxIV, either due to disorder of Cys170 and surrounding residues in the helix α6 region, or due to disulfide bond reduction by electron flux during data collection.

Crystal structure of conoidin A bound to AcePrx-1

To obtain a direct view of the inactivated enzyme, we determined the crystal structure of AcePrx-1/conoidin A complex. Crystals of the Δ171/conoidin A complex produced clearer electron density in the active site region than crystals of the wild type AcePrx-1/conoidin A complex, suggesting that the disordered C-terminal tail has a destabilizing effect on the active site region. The Δ171/conoidin A complex was prepared from fully reduced Δ171 protein as described in the Experimental Procedures. The protein in the conoidin A complex had an essentially identical structure to the unliganded structure, with an RMSD of 0.43 Å in the Cα positions of the two structures. Although the 3.0 Å resolution crystal structure of the complex contained only five AcePrx-1 monomers in the asymmetric unit, decameric rings are generated by the crystallographic symmetry. An F_o-F_c electron density difference map revealed positive electron density across the dimer interface that was connected to Cys49 in two of the five subunits (Figure 6C-D). Based on our LC-ESI-MS data, the electron density is expected to represent an average of QDO, QMO, and Qx adducts. The first adduct, between Cys49 of subunit B and Cys170 of subunit A, was modeled as QMO (Figure 6C-D), because the oxygen atom at the N4 N-oxide oxygen of QDO or Qx adducts caused a steric clash with His91 of a symmetry-related AcePrx-1 molecule. The second adduct, which connects Cys49 on subunit C to Cys170 on subunit D, could be modeled as QDO without steric clashes from neighboring molecules. The electron density was weaker for the second adduct, which was refined with an occupancy of 0.5. SDS-PAGE of dissolved AcePrx-1/conoidin A crystals confirmed that the protein was fully crosslinked by the inhibitor (Figure 3C). We conclude that the low apparent occupancy is due to conformational flexibility (thermal disorder) of the adduct. Moreover, the relative orientation of the two modeled adducts to the dimer dyad differs by nearly 90°. Overall, the different structure of the two conoidin A adducts, along with the weak or absent electron density for adducts in four out of five subunits, suggest that the adducts have substantial conformational flexibility in the context of the locally-unfolded active site.

Discussion

Hookworms have devastating effects on global health and new anthelminthic treatments are needed. Peroxiredoxins are emerging as central players in parasite biology by performing various essential functions in hookworms and other parasites including antioxidant protection, intracellular signaling through ROS, protein folding, and immunomodulation. The diversity of these functions suggests that peroxiredoxins are promising potential targets for anti-parasite therapeutics.

We have shown here that AcePrx-1 is a peroxidase that is partially secreted by adult *A. ceylanicum* hookworms. The crystal structure of AcePrx-1 shows that it is most similar to human PrxIV, despite the presence of an N-terminal extension including a signal peptide in PrxIV but not AcePrx-1 (Cao, et al., 2011). The absence of the signal peptide in AcePrx-1 raises the possibility that it is exported through a non-classical secretory pathway, as previously proposed for certain secretory products in the helminthic parasite *F. hepatica* (Robinson, et al., 2009). Notably, Prxs secreted by *F. hepatica* and *S. mansoni* have recently been proposed to activate macrophages and promote Th2 helper cell differentiation through expression of the chitinase-like protein Ym1 (Donnelly, et al., 2010). Whether secreted AcePrx-1 also has immunomodulatory activity remains to be determined.

Conoidin A, which was previously identified as an inhibitor of TgPrxII, also inhibits AcePrx-1 consumption of peroxide in a dose-dependent manner; the monobrominated analog conoidin B does not show significant inhibition. Conoidins A and B inhibit human peroxiredoxins hPrxII and hPrxIV with similar efficiency, indicating that selectivity remains an issue to be addressed by further chemical optimization of conoidin A or identification of new, more selective ligands. Also, prior to embarking on compound optimization it is necessary to prove that enzyme is essential and its cell function is not redundant.

Our mass spectrometry data show that conoidin A can inhibit AcePrx-1 by alkylating or crosslinking the catalytic cysteines (Figure 4D), and possibly by oxidizing the resolving cysteine. We note that oxidation and alkylation (or crosslinking) are not mutually exclusive. Conoidin A is expected to inhibit other 2-Cys peroxiredoxins, including mammalian homologs, by the same mechanisms.

The pK_a value of the peroxidatic cysteine ranges from 5–6 for typical 2-Cys peroxiredoxins (Nelson, et al., 2008; Ogusucu, et al., 2007; Peskin, et al., 2007). Three conserved residues in the active site have been proposed to lower the pKa of the peroxidatic cysteine in other peroxiredoxins: arginine and threonine residues that are presumed to stabilize the thiolate anion, and a proline that shields the active site from water (Nelson, et al., 2008; Ogusucu, et al., 2007; Peskin, et al., 2007). In addition to these features, analysis of the AcePrx-1 structure reveals that Cys49 and Cys170 are positioned at the positive end of the electrical macrodipole of helix α2, providing an additional mechanism for lowering the pK_a (or, in the disulfide-linked form, increasing electronegativity) of these residues. We propose that the unusually low pK_a of the peroxidatic cysteine makes the side chain highly reactive to conoidin A at physiological pH by maintaining it in the more nucleophilic thiolate state. Similarly, in the locally unfolded conformation, the resolving cysteine is also near the helix α2 macrodipole.

We conclude that the primary mechanism of inhibition of AcePrx-1 is alkylation of either Cys49 or Cys170 or both (Figure 4D). Hyperoxidation of Cys170 cannot be ruled out as a mechanism of inhibition but is likely to play a minor role under physiological conditions. Although sulfiredoxin (Srx) can repair sulfinic acid oxidation of Cys49, the active site pocket in Srx specifically accommodates only the Prx peroxidatic cysteine and a molecule of ATP but not the resolving cysteine (Jonsson, et al., 2009). Thus, oxidation of Cys170 to

sulfenic (or sulfinic or sulfonic) acid abolishes its ability to regenerate the active enzyme via intermolecular disulfide formation, and hyperoxidation of Cys170 inactivates 2-Cys peroxiredoxins. Since these hyperoxidation and alkylation mechanisms can occur simultaneously, their effects on enzyme activity are expected to be additive. This is supported by the reduced inhibitory activity of a deoxygenated conoidin A derivative against TgPrxII (Liu, et al., 2010).

The crystal structure of AcePrx-1 bound to conoidin A provides a direct view of the conoidin A adduct crosslinking the active site cysteines and validates our proposed mechanism of conoidin inhibition. Oxidation of Cys49 by conoidin A, like natural oxidation during catalysis (Hall, et al., 2009), converts the enzyme from the fully folded to the locally unfolded conformation. The C-terminal tail (residues 171-196) becomes disordered in the locally unfolded conformation, and the active site cysteines are brought within disulfide bonding distance, whereas they are 4 Å further apart in the fully folded state of hPrxIV. The C-terminal tail is the region with the lowest sequence conservation across peroxiredoxins from different species. A few conserved residues in the C-terminal tail stabilize the active site cysteines in their respective pockets in the fully folded state. The remaining amino acid sequence is poorly conserved between human and hookworm enzymes. Hence, a possible strategy for increasing the species specificity of conoidin A for hookworm peroxiredoxins is to functionalize the aromatic system of conoidin to preferentially react (or interact) with hookworm-specific amino acids within the C-terminal tail. For example, an amine reactive group could be appropriately placed to react with the reactive amine group of Lys178, which is specific to parasitic nematode Prx sequences (Figure 1).

Our observation that AcePrx-1 is predominately expressed in adult hookworms and not in egg or larval stages suggests that inhibition of egg hatching by conoidin A (Treger, et al., 2013) may occur through inhibition of a protein other than AcePrx-1. A second peroxiredoxin has been identified in *A. ceylanicum* but its expression pattern and biochemical activity have not yet been studied. In validating peroxiredoxins as potential drug targets, it will be important to establish the specific functional roles of each peroxiredoxin, and of any related enzymes in each of the developmental stages of the hookworm.

Significance

In summary, our structural, biophysical and biochemical analysis of AcePrx-1 extends our understanding of the mechanism of inhibition by conoidin A. We have shown that conoidin A inactivates AcePrx-1 and its human orthologs hPrxII and hPrxIV by alkylating or crosslinking the catalytic cysteines, and that irreversible oxidation of the resolving cysteine by conoidin A may contribute additional inhibitory activity. Our crystal structure of oxidized AcePrx-1 shows that it forms stable disulfide-linked decamers like its closest structural homolog hPrxIV, but unlike other 2-Cys peroxiredoxins. A helix macrodipole near the active site increases the reactivity of the catalytic cysteine residues to conoidin A. The biochemical and structural characterization of AcePrx-1 presented here provides a framework for the validation of AcePrx-1 as a potential drug target and for the identification of new candidate targets to combat hookworm infection. Moreover, this study suggests that conoidin compounds could serve as chemical probes to explore the emerging functions of peroxiredoxins in protein folding and immunomodulation by human parasites.

Experimental Procedures

Small molecule inhibitors

Conoidin A (2,3-bis(bromomethyl)-quinoxaline-1,4-dioxide) and its monobrominated analog conoidin B (2-(bromomethyl)-3-methylquinoxaline-1,4-dioxide) were kindly provided by the NIH Chemical Genomics Center or purchased from Sigma-Aldrich.

Human peroxiredoxin proteins

The pQTEV-PRDX2 vector expressing hPrxII was purchased from Addgene (plasmid #31338). hPrxII was purified using the same protocol as for AcePrx-1. The N-terminal histidine purification tag was not cleaved for activity assays. hPrxIV was purchased from United States Biological Corp.

Cloning of Ancylostoma ceylanicum peroxiredoxin 1

Complementary DNA (cDNA) was synthesized from total adult hookworm RNA for use in PCR and RTPCR reactions to amplify the AcePrx-1 sequence and assess mRNA transcript abundance within developmental stages of *A. ceylanicum* using the iScript™ cDNA synthesis kit (BioRad). The complete open reading frame (ORF) of AcePrx-1 was amplified by PCR using oligonucleotide primers modified to contain an N-terminal histidine affinity purification tag. The amplified gene was then subcloned into pET11 using NdeI and BamHI restriction sites for expression in *E. coli*. Cysteine mutants and deletion mutants were generated by site-directed mutagenesis or overlap extension PCR.

Real-time PCR analysis of AcePrx-1 transcript abundance

AcePrx-1 mRNA transcript levels were quantified by RT-PCR in cDNA populations obtained from eggs/L1, infectious L3, and adult male and female worms. Primers amplifying a ~100 base pair section of the ORF were generated with Primer Express (Applied Biosystems). PCR amplification was performed in a 96-well format using optical tube strips and caps in an MJ Research DNA Engine Opticon 2 PCR apparatus (BioRad) and iQ™ SYBR® Green Supermix. Reactions were cycled under the following conditions: 95°C for 15 min, followed by 15 s at 95°C and 60 s at 60°C. To confirm the absence of non-specific amplification in PCR reactions, control samples containing water substituted for template were run and a melting point dissociation curve was generated after every experiment to confirm the presence of a single PCR amplicon in all experimental wells. All data were analyzed with Opticon Monitor™ version 3.1 (BioRad). A comparative cycle threshold method was used to obtain quantitative values for transcript levels in all samples.

Expression and purification of wild type and mutant AcePrx-1 proteins

The AcePrx-1 expression vectors were transformed into *Escherichia coli* BL21 (DE3) strain (Novagen) and cultured in Luria Broth supplemented with ampicillin at 0.1 mg/ml. Cells were induced during log-phase growth with 0.4 mM IPTG for 4 h at 37°C. AcePrx-1 yield was 40-80 mg per liter of cell culture.

AcePrx-1 was purified by nickel-affinity and size-exclusion chromatography. Cells were lysed at 4°C in lysis buffer, 50 mM HEPES pH 7.5, 0.1 M NaCl, 2 mM DTT. After centrifugation for 40 min at 40,000 rpm the clarified cell lysate was loaded onto a HisTrap HP nickel-affinity column (GE Healthcare). AcePrx-1 eluted off the column at 0.15 M imidazole pH 8.0. AcePrx-1 was further purified on a Superdex 200 size-exclusion column (GE Healthcare) in 10 mM HEPES pH 7.5, 0.1 M NaCl, 10 mM DTT. AcePrx-1 mutants were purified using the same procedure. The N-terminal histidine tag was not cleaved after purification.

Generation of a α-AcePrx-1 antibody and detection of AcePrx-1 in hookworm extracts

Groups of Golden Syrian hamsters (*Mesocricetus auratus*) were immunized with 100 μg of rAcePrx-1 emulsified in Freund's Complete adjuvant (Sigma). The hamsters were boosted twice at three week intervals with an additional 50 μg of protein emulsified in Freund's incomplete adjuvant (Sigma). Hamsters were sacrificed and serum was collected 10 days after the third and final vaccination, and the IgG fraction was purified by Protein G affinity chromatography.

The presence of native AcePrx-1 in soluble protein extracts of *A. ceylanicum* eggs (E), early larvae (L1), infectious larvae (L3), adult male/female worm extract (HEX), and secreted proteins from adult worms (ES) was assessed by immunoblot as previously described (Cho, et al., 2007). Nitrocellulose membranes containing native hookworm protein preparations were probed with the hamster α-rAcePrx-1 IgG (1:3000 dilution), followed by a secondary horseradish peroxidase-conjugated goat α-hamster IgG (1:3000 dilution).

Peroxiredoxin activity assay

Reduction of peroxide (H_2O_2) by recombinant AcePrx-1, hPrxII, and hPrxIV was measured using the PEROXsay assay kit (G-Biosciences), which monitors the oxidation of ferrous (Fe^{2+}) ions to ferric (Fe^{3+}) ions by H_2O_2. Reactions were performed at 25°C in 50 mM sodium phosphate, pH 7.4, 0.2 mM DTT. After incubation of 2 μM peroxiredoxin with 40 μM H_2O_2 for 20 min, the enzymatic reaction was quenched with the assay solution (containing D-sorbitol, xylenol orange, ferric ammonium sulfate, and sulfuric acid) and incubated for an additional 30 min. Absorbance was measured at 595 nm on a microplate reader (Biotek). A mutant lacking the active site cysteines was used as a negative control. A H_2O_2 titration standard curve in the absence of enzyme was used to calculate the amount of H_2O_2 consumed in each assay. One activity unit was defined as the amount of enzyme required to reduce 1 μmol of H_2O_2 per minute.

Assays of peroxiredoxin inhibition by conoidin compounds were performed as described above except with 1 U of each enzyme pre-incubated with various concentrations of conoidin A or conoidin B (0-120 μM) for 30 min at 25°C before addition of H_2O_2. The triple cysteine mutant was used to normalize each concentration to 100% inhibition. All assays were performed in triplicate.

AcePrx-1 crosslinking assay

Wild type and mutant AcePrx-1 proteins were desalted on a HiTrap desalting column (GE Healthcare) to remove excess DTT and immediately reacted with a 3-fold molar excess of conoidin A for 0.5–96 h at 25°C. The final concentration of AcePrx-1 in the crosslinking reaction was 0.8 g/l, in 10 mM HEPES, 0.1 M NaCl. The sample was analyzed by SDS-PAGE in the presence or absence of 0.2 M DTT.

Liquid chromatography and electrospray ionization mass spectrometry (LC-ESI-MS)

Samples from the crosslinking assay (after various incubation times up to 24 h) were injected on a Waters ACQUITY Ultraperformance liquid chromatography system coupled to an ACQUITY UPLC Photodiode Array eλ detector. Electrospray mass spectrograms were collected in the positive ion mode and subsequently deconvoluted for molecular weight determination with MASSLYNX software (Waters).

Crystallization and structure determination of AcePrx-1

Crystals were grown by hanging drop vapor diffusion from a 3.6 g/l solution of AcePrx-1 at 12°C. For each drop, 1 μl of AcePrx-1 in 10 mM HEPES pH 7.5, 0.1 M NaCl was mixed

with 0.5 μl of the reservoir solution, 6-8% PEG3350, 0.1 M MES pH 6.0. Crystals were flash frozen in liquid nitrogen in reservoir solution supplemented with 20% glycerol. Crystallographic data were collected at 100 K and processed with HKL (Otwinowski and Minor, 1997). Crystals belonged to space group $P2_1$ with ten molecules per asymmetric unit. The structure of AcePrx-1 was determined by molecular replacement with Phaser (McCoy, et al., 2007) using a single subunit of human PrxII (PDB code 1QMV (Schroder, et al., 2000)) as the search model. The atomic coordinates and temperature factors were refined with REFMAC5 (Murshudov, et al., 1997), initially with non-crystallographic symmetry restraints applied to all ten subunits. The atomic model was improved with cycles of model building with COOT (Emsley and Cowtan, 2004) followed by positional refinement. Rigid-body motions of the ten subunits were modeled with REFMAC5 in terms of TLS tensors for translation, libration, and screw-rotation (Winn, et al., 2001). Water molecules were added using an automated procedure in COOT and by visual inspection.

Crystals of AcePrx-1 Δ171 in complex with conoidin A were obtained from fully reduced Δ171 protein (1 g/l), which was desalted to remove excess DTT and immediately reacted at a 3:1 molar ratio with conoidin A (150 μM). The reaction was monitored to completion by mass spectrometry. Co-crystals of the protein-inhibitor complex were grown by hanging drop vapor diffusion as described above for unliganded AcePrx-1 but with 1-2% PEG3350, 0.1 M MES pH 6.0 as the precipitant, and reservoir solution supplemented with 30% glycerol as the cryoprotectant. The conoidin A stock solution was in 100% DMSO, and the final concentration of DMSO in protein solutions was less than 0.1%. Crystals belonged to space group C*2* with five molecules per asymmetric unit. The structure was determined by molecular replacement with Phaser using an AcePrx-1 pentamer as the search model. The atomic coordinates were first refined in REFMAC as a rigid body, revealing additional density at the C-termini and connected to the peroxidatic cysteine residue on two of the five subunits in $2F_o - F_c$ and $F_o - F_c$ difference Fourier maps. The quinoxaline dioxide adduct bearing sulfur thiols in place of the bromine atoms was generated using PRODRG and input into SKETCHER to create the ligand library description for use in refinement. See Table 1 for complete data collection and refinement statistics.

Supplementary Material

Refer to Web version on PubMed Central for supplementary material.

Acknowledgments

We thank staff at beamline 24-ID-E of the Northeastern Collaborative Access Team at the Advanced Photon Source (APS) of the Argonne National Laboratory, and at the X25 and X29A beamlines of the National Synchrotron Light Source (NSLS) at Brookhaven National Laboratory. We thank Lisa Harrison for critical reading of manuscript. We acknowledge Alanna Schepartz for use of her mass spectrometer and Tae Han Kim for advice on chemical mechanisms. This work was supported by a Burroughs Wellcome Investigator Award and NIH grant P01 GM022778 to YM, and NIH grant K22 AI08476 to JJV. JBN was supported in part by NIH training grant T32 GM08283. Use of the APS and NSLS is supported by the Offices of Biological and of Basic Energy Sciences of the US Department of Energy.

References

Albonico M, Engels D, Savioli L. Monitoring drug efficacy and early detection of drug resistance in human soil-transmitted nematodes: a pressing public health agenda for helminth control. Int J Parasitol. 2004; 34:1205–1210. [PubMed: 15491582]

Awasthi S, Bundy DA, Savioli L. Helminthic infections. BMJ. 2003; 327:431–433. [PubMed: 12933732]

Bundy D, Sher A, Michael E. Good worms or bad worms: do worm infections affect the epidemiological patterns of other diseases? Parasitol Today. 2000; 16:273–274. [PubMed: 10858643]

Bungiro R, Cappello M. Twenty-first century progress toward the global control of human hookworm infection. Curr Infect Dis Rep. 2011; 13:210–217. [PubMed: 21462001]

Cao Z, Bhella D, Lindsay JG. Reconstitution of the mitochondrial PrxIII antioxidant defence pathway: general properties and factors affecting PrxIII activity and oligomeric state. J. Mol. Biol. 2007; 372:1022–1033. [PubMed: 17707404]

Cao Z, Tavender TJ, Roszak AW, Cogdell RJ, Bulleid NJ. Crystal structure of reduced and of oxidized peroxiredoxin IV enzyme reveals a stable oxidized decamer and a non-disulfide-bonded intermediate in the catalytic cycle. J Biol Chem. 2011; 286:42257–42266. [PubMed: 21994946]

Cho Y, Jones BF, Vermeire JJ, Leng L, DiFedele L, Harrison LM, Xiong H, Kwong YK, Chen Y, Bucala R, et al. Structural and functional characterization of a secreted hookworm Macrophage Migration Inhibitory Factor (MIF) that interacts with the human MIF receptor CD74. J Biol Chem. 2007; 282:23447–23456. [PubMed: 17567581]

Donnelly S, O'Neill SM, Stack CM, Robinson MW, Turnbull L, Whitchurch C, Dalton JP. Helminth cysteine proteases inhibit TRIF-dependent activation of macrophages via degradation of TLR3. J Biol Chem. 2010; 285:3383–3392. [PubMed: 19923225]

Emsley P, Cowtan K. Coot: model-building tools for molecular graphics. Acta Crystallogr D Biol Crystallogr. 2004; 60:2126–2132. [PubMed: 15572765]

Geiger SM, Massara CL, Bethony J, Soboslay PT, Correa-Oliveira R. Cellular responses and cytokine production in post-treatment hookworm patients from an endemic area in Brazil. Clin. Exp. Immunol. 2004; 136:334–340. [PubMed: 15086399]

González M, Cerecetto H, Monge A. Quinoxaline 1,4-Dioxide and Phenazine 5,10-Dioxide. Chemistry and Biology. Top Heterocycl Chem. 2007; 11:179–211.

Hall A, Karplus PA, Poole LB. Typical 2-Cys peroxiredoxins--structures, mechanisms and functions. Febs J. 2009; 276:2469–2477. [PubMed: 19476488]

Haraldsen JD, Liu G, Botting CH, Walton JG, Storm J, Phalen TJ, Kwok LY, Soldati-Favre D, Heintz NH, Muller S, et al. Identification of Conoidin a as a Covalent Inhibitor of Peroxiredoxin Ii. Org Biomol Chem. 2009; 7:3040–3048. [PubMed: 21359112]

Hofmann B, Hecht HJ, Flohe L. Peroxiredoxins. Biol Chem. 2002; 383:347–364. [PubMed: 12033427]

Hotez PJ, Brooker S, Bethony JM, Bottazzi ME, Loukas A, Xiao S. Hookworm infection. N Engl J Med. 2004; 351:799–807. [PubMed: 15317893]

Humphries D, Nguyen S, Boakye D, Wilson M, Cappello M. The promise and pitfalls of mass drug administration to control intestinal helminth infections. Curr. Opin. Infect. Dis. 2012; 25:584–589. [PubMed: 22903231]

Jang HH, Lee KO, Chi YH, Jung BG, Park SK, Park JH, Lee JR, Lee SS, Moon JC, Yun JW, et al. Two enzymes in one; two yeast peroxiredoxins display oxidative stress-dependent switching from a peroxidase to a molecular chaperone function. Cell. 2004; 117:625–635. [PubMed: 15163410]

Jonsson TJ, Johnson LC, Lowther WT. Protein engineering of the quaternary sulfiredoxin.peroxiredoxin enzyme.substrate complex reveals the molecular basis for cysteine sulfinic acid phosphorylation. J Biol Chem. 2009; 284:33305–33310. [PubMed: 19812042]

Keiser J, Utzinger J. Efficacy of current drugs against soil-transmitted helminth infections: systematic review and meta-analysis. JAMA. 2008; 299:1937–1948. [PubMed: 18430913]

Liu G, Botting CH, Evans KM, Walton JA, Xu G, Slawin AM, Westwood NJ. Optimisation of conoidin A, a peroxiredoxin inhibitor. ChemMedChem. 2010; 5:41–45. [PubMed: 19946931]

Loukas A, Constant SL, Bethony JM. Immunobiology of hookworm infection. FEMS Immunol. Med. Microbiol. 2005; 43:115–124. [PubMed: 15681140]

Maizels RM, Yazdanbakhsh M. Immune regulation by helminth parasites: Cellular and molecular mechanisms. Nat. Rev. Immunol. 2003; 3:733–744. [PubMed: 12949497]

McCoy AJ, Grosse-Kunstleve RW, Adams PD, Winn MD, Storoni LC, Read RJ. Phaser crystallographic software. J. Appl. Cryst. 2007; 40:658–674. [PubMed: 19461840]

Murshudov GN, Vagin AA, Dodson EJ. Refinement of macromolecular structures by the maximum-likelihood method. Acta Crystallogr D Biol Crystallogr. 1997; 53:240–255. [PubMed: 15299926]

Nelson KJ, Knutson ST, Soito L, Klomsiri C, Poole LB, Fetrow JS. Analysis of the peroxiredoxin family: using active-site structure and sequence information for global classification and residue analysis. Proteins. 2011; 79:947–964. [PubMed: 21287625]

Nelson KJ, Parsonage D, Hall A, Karplus PA, Poole LB. Cysteine pK(a) values for the bacterial peroxiredoxin AhpC. Biochemistry. 2008; 47:12860–12868. [PubMed: 18986167]

Ogusucu R, Rettori D, Munhoz DC, Netto LE, Augusto O. Reactions of yeast thioredoxin peroxidases I and II with hydrogen peroxide and peroxynitrite: rate constants by competitive kinetics. Free Radic Biol Med. 2007; 42:326–334. [PubMed: 17210445]

Onyemelukwe GC, Musa BO. T-lymphocyte subsets in patients with hookworm infection in Zaria, Nigeria. Afr J Med Med Sci. 2001; 30:255–259. [PubMed: 14510099]

Otwinowski Z, Minor W. Processing of X-ray Diffraction Data Collected in Oscillation Mode. Methods Enzymol. 1997; 276:307–326.

Park SH, Chung YM, Lee YS, Kim HJ, Kim JS, Chae HZ, Yoo YD. Antisense of human peroxiredoxin II enhances radiation-induced cell death. Clin Cancer Res. 2000; 6:4915–4920. [PubMed: 11156252]

Peskin AV, Low FM, Paton LN, Maghzal GJ, Hampton MB, Winterbourn CC. The high reactivity of peroxiredoxin 2 with H(2)O(2) is not reflected in its reaction with other oxidants and thiol reagents. J Biol Chem. 2007; 282:11885–11892. [PubMed: 17329258]

Robinson MW, Menon R, Donnelly SM, Dalton JP, Ranganathan S. An integrated transcriptomics and proteomics analysis of the secretome of the helminth pathogen Fasciola hepatica: proteins associated with invasion and infection of the mammalian host. Mol Cell Proteomics. 2009; 8:1891–1907. [PubMed: 19443417]

Roussilhon C, Brasseur P, Agnamey P, Perignon JL, Druilhe P. Understanding human-Plasmodium falciparum immune interactions uncovers the immunological role of worms. PLoS One. 2010; 5:e9309. [PubMed: 20174576]

Saccoccia F, Di Micco P, Boumis G, Brunori M, Koutris I, Miele AE, Morea V, Sriratana P, Williams DL, Bellelli A, et al. Moonlighting by different stressors: crystal structure of the chaperone species of a 2-cys peroxiredoxin. Structure. 2012; 20:429–439. [PubMed: 22405002]

Schroder E, Littlechild JA, Lebedev AA, Errington N, Vagin AA, Isupov MN. Crystal structure of decameric 2-Cys peroxiredoxin from human erythrocytes at 1.7 A resolution. Structure. 2000; 8:605–615. [PubMed: 10873855]

Tavender TJ, Sheppard AM, Bulleid NJ. Peroxiredoxin IV is an endoplasmic reticulum-localized enzyme forming oligomeric complexes in human cells. Biochem J. 2008; 411:191–199. [PubMed: 18052930]

Tavender TJ, Springate JJ, Bulleid NJ. Recycling of peroxiredoxin IV provides a novel pathway for disulphide formation in the endoplasmic reticulum. Embo J. 2010; 29:4185–4197. [PubMed: 21057456]

Toh SQ, Glanfield A, Gobert GN, Jones MK. Heme and blood-feeding parasites: friends or foes? Parasit Vectors. 2010; 3:108. [PubMed: 21087517]

Treger RS, Otchere J, Keil MF, Quagraine JE, Rai G, Mott BT, Humphries DL, Wilson M, Cappello M, Vermeire JJ. In vitro Screening of Compounds against Laboratory and Field Isolates of Human Hookworm Reveals Quantitative Differences in Anthelminthic Susceptibility. Am J Trop Med Hyg. 2013 in press.

Winn MD, Isupov MN, Murshudov GN. Use of TLS parameters to model anisotropic displacements in macromolecular refinement. Acta Crystallogr D Biol Crystallogr. 2001; 57:122–133. [PubMed: 11134934]

Winterbourn CC. Reconciling the chemistry and biology of reactive oxygen species. Nat Chem Biol. 2008; 4:278–286. [PubMed: 18421291]

Wood ZA, Poole LB, Hantgan RR, Karplus PA. Dimers to doughnuts: redox-sensitive oligomerization of 2-cysteine peroxiredoxins. Biochemistry. 2002; 41:5493–5504. [PubMed: 11969410]

Zito E, Melo EP, Yang Y, Wahlander A, Neubert TA, Ron D. Oxidative protein folding by an endoplasmic reticulum-localized peroxiredoxin. Mol Cell. 2010; 40:787–797. [PubMed: 21145486]

Highlights

- Hookworms rely on peroxiredoxins as antioxidants and for intracellular signaling
- Peroxiredoxin-1 expressed in adult hookworms is covalently inactivated by conoidin A
- Hookworm Prx-1 is a decamer and has a structure similar to human peroxiredoxin IV
- Conoidin A may be useful to validate peroxiredoxins as anthelminthic drug targets

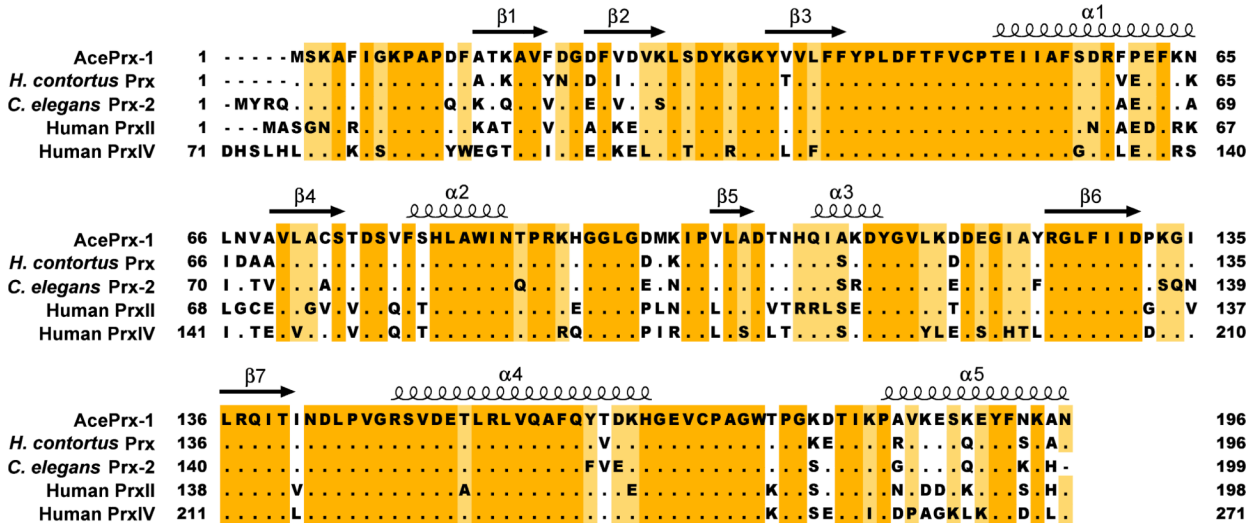

Figure 1. Sequence alignment of peroxiredoxin sequences

Genbank IDs are JX124321 (*Ancylostoma ceylanicum* Prx-1), 47499100 (*Haemonchus contortus* Prx), 193204376 (*Caenorhabditis elegans* Prx-2), 32189392 (human PrxII) and 5453549 (human PrxIV). Secondary structure elements in the AcePrx-1 crystal structure are overlaid on the alignment.

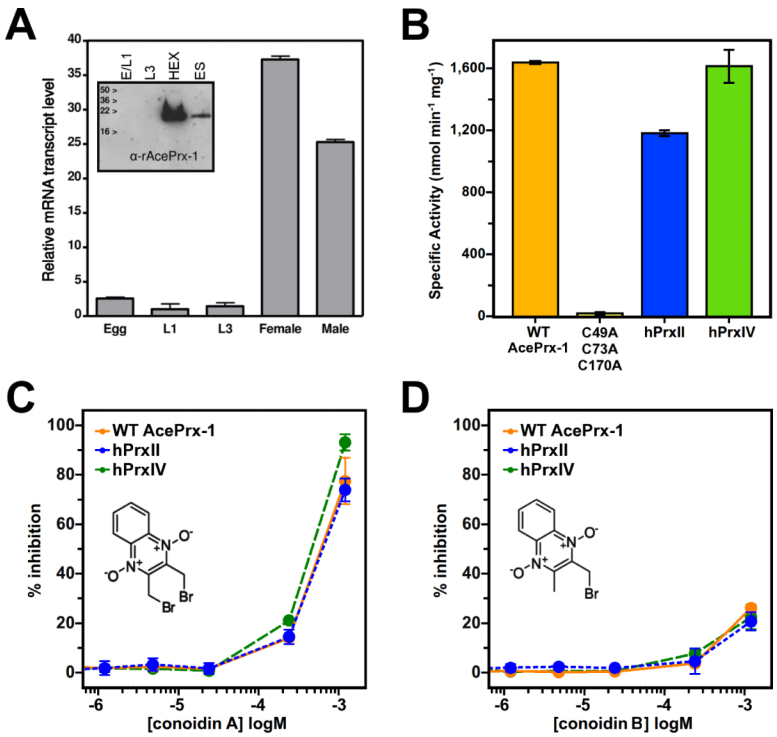

Figure 2. AcePrx-1 is expressed in adult hookworms and is inhibited by conoidin A

A. Analysis of AcePrx-1 mRNA levels and protein expression throughout the life cycle of *A. ceylanicum* shows that AcePrx-1 is highly expressed in adult hookworms compared to egg (E), early larval stage (L1) or infectious larvae (L3).

B. Specific activity of AcePrx-1 as determined by monitoring the consumption of H_2O_2 in an iron-based colorimetric assay. Activity of human peroxiredoxins-II and -IV are provided for comparison, with the C49A/C73A/C170A AcePrx-1 mutant used as a negative control.

C-D. Inhibition of AcePrx-1, hPrxII, and hPrxIV activity by conoidin A (C) and conoidin B (D). The lack of inhibitory activity of conoidin B in the concentration range assayed may be due in part to the low solubility of conoidin B.

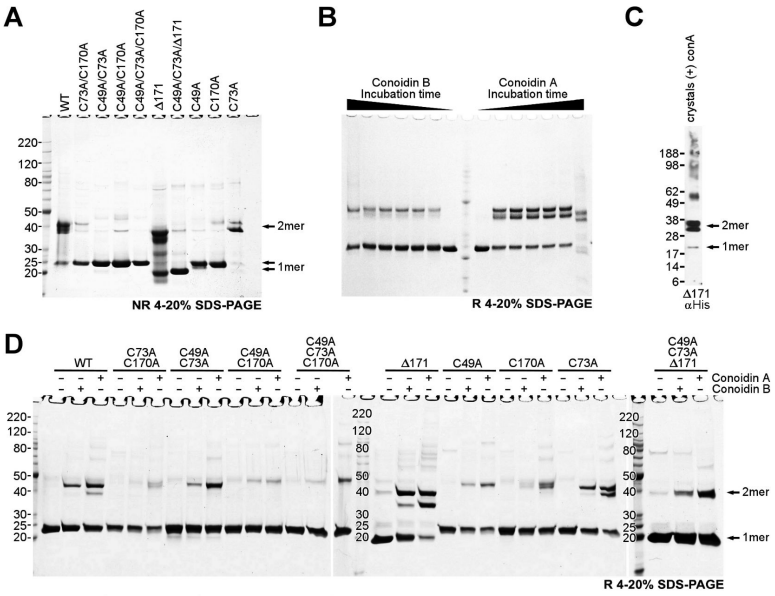

Figure 3. SDS-PAGE analysis shows that both conoidin A and conoidin B react with AcePrx-1

AcePrx-1 was purified under reducing conditions and desalted immediately prior to sample preparation. A. Wild type and mutant AcePrx-1 under non-reducing conditions. Most of the wild type protein is a disulfide-linked dimer. Neither a C73A mutation nor a deletion of C-terminal residues 172-196 affect dimerization. Mutation of Cys49 or Cys170 renders the protein predominantly monomeric.

B. Time course assay of wild type AcePrx-1 reactivity with conoidin A and conoidin B. The time points are 0 h, 0.5 h, 1 h, 3 h, 6 h, 24 h and 96 h. The samples were boiled in Laemmli buffer to quench reactivity, and then run under reducing conditions. Dimeric species appear within only 0.5 h and remain stable. After 96 h, appreciable degradation was observed in these samples in the presence of conoidin A but not of conoidin B over the same duration. Faint bands corresponding to higher-order oligomers were observed after 96 h.

C. Reducing gel from dissolved crystals of the AcePrx-1(Δ171)/conoidin A complex. Conidin A covalently crosslinks AcePrx-1 into dimers. Traces of monomer and higher order oligomers are visible.

D. Reducing gel showing that conoidin A and conoidin B cause covalent (or non-covalent SDS-resistant) oligomerization of wild type and mutant AcePrx-1 after incubation for 24 h. The appearance of higher-order oligomer bands in the C49A/C73A/C170A triple mutant suggest that side chains other than cysteine can react with conoidin A nonspecifically and lead to crosslinking of AcePrx-1. See also Table S1.

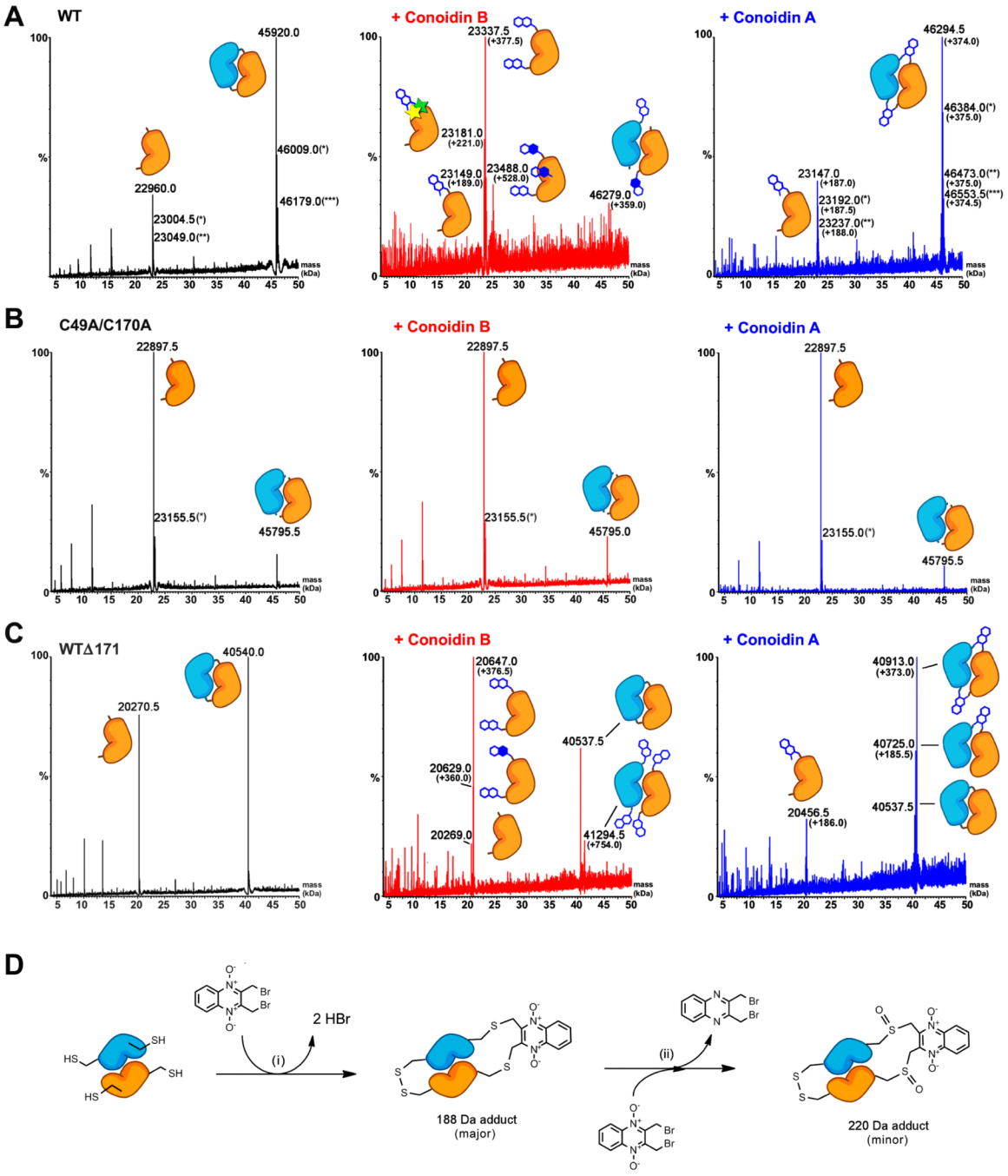

Figure 4. Conoidin A and conoidin B covalently modify AcePrx-1 by alkylation or crosslinking

Liquid chromatography and electrospray ionization mass spectra (LC-ESI-MS) of wild type and mutant AcePrx-1 are shown without pretreatment (left column), after treatment with conoidin B (middle column) and after treatment with conoidin A (right column). The chemical composition of any adducts is shown schematically next to each peak in the spectra. Quinoxaline dioxide (QDO) adducts are represented as two open hexagons. Filled hexagons indicate deoxygenation to the mono-oxide. Each star represents addition of a single oxygen to the protein.

A. Spectra for wild type AcePrx-1 after a 6-h treatment. Wild type AcePrx-1 is predominately dimeric with a mass of 45,920 Da. Additional peaks represent the monomer

(22,960 Da) and various other protonation states, indicated by asterisks. Conoidin B treatment results in alkylation of up to three sites on the monomer, while conoidin A treatment results in alkylation with a single QDO adduct, or crosslinking by two QDO adducts.

B. The C49A/C170A double mutant does not react with conoidin A or conoidin B, even after treatment for 24 h (shown here), suggesting that the catalytic cysteine residues are the specific sites of modification in AcePrx-1.

C. A C-terminal deletion mutant with residues 172-196 missing produces a very similar set of adducts to wild type AcePrx-1 (24-h conoidin A/B treatment shown here).

D. Proposed mechanism of conoidin A inhibition of AcePrx-1. A peroxiredoxin dimer (orange and blue), drawn schematically in its fully folded conformation undergoes successive S_N2 reactions with a single molecule of conoidin A, (i), to generate a 188-Da crosslinked adduct. An additional minor product is formed by oxidation of the thioether moieties by the N-oxide on conoidin A, (ii), which produces the 220 Da covalent adduct observed in our mass spectrometry experiments. See also Figure S1.

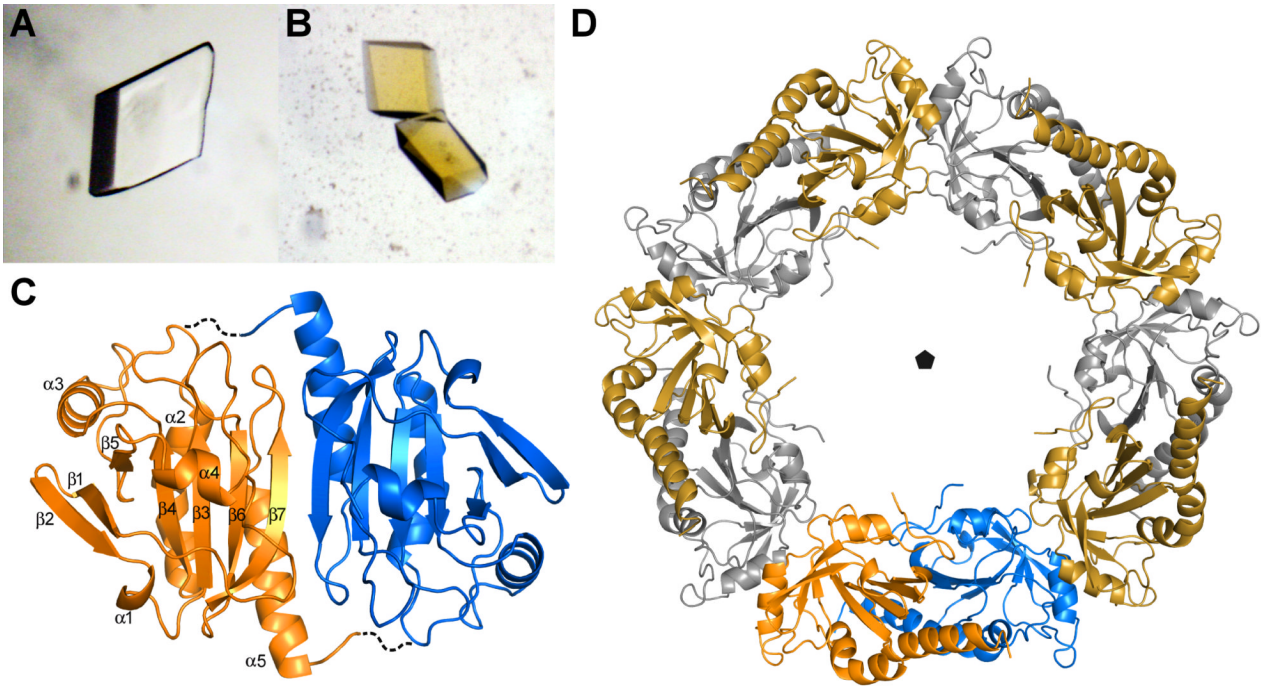

Figure 5. Crystal structure of AcePrx-1

A. Crystals of AcePrx-1 are colorless in the absence of conoidin A.

B. AcePrx-1 crystals grown in the presence of conoidin A are yellow, suggesting that conoidin A binds to the enzyme.

C. AcePrx-1 adopts a fold similar to other peroxiredoxins. The most similar structure is human Prx-4 (PDB code 3TJB). AcePrx-1 forms dimers principally via inter-strand contacts to form an eight-stranded β-sheet. Dashed lines connect the active site cysteines across the dimer interface.

D. Five AcePrx-1 dimers assemble into a decamer in solution and in the crystal structure. See also Figure S2.

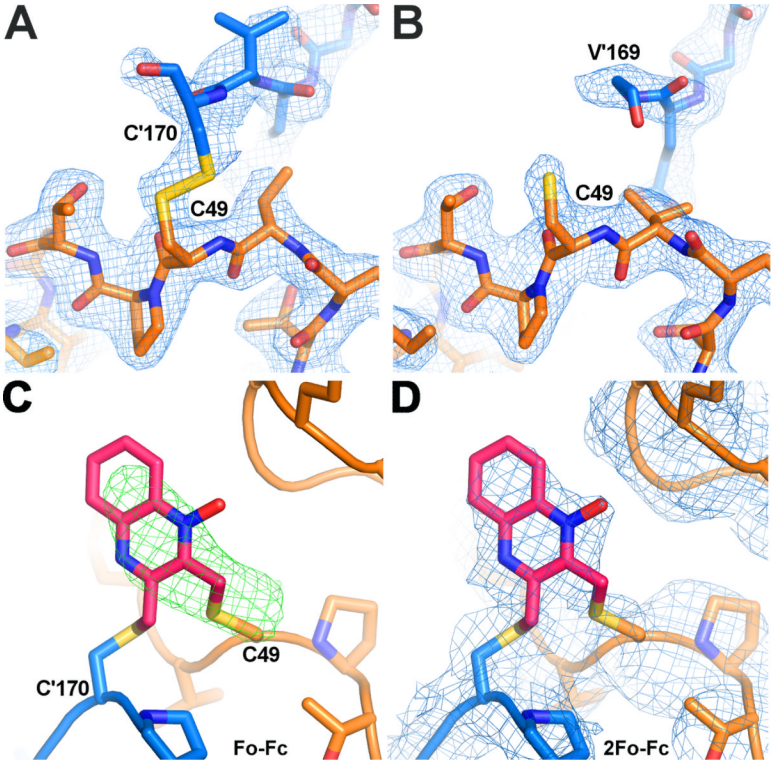

Figure 6. The active site of AcePrx-1 in the presence and absence of conoidin A

A. The structure of AcePrx-1 shows that the enzyme is in the locally unfolded conformation, with disulfide bonds between the peroxidatic and resolving cysteine residues (Cys49 and Cys170, respectively) visible in two of the ten active sites in the decameric asymmetric unit (B, C). Subunits A (blue) and B (orange) are shown.

B. In the remaining subunits (A, D-J), Cys170 is disordered and electron density is lacking for the disulfide bond and helix α6 (subunit E is in orange).

C. Positive electron density is present in F_o - F_c maps (green) near the active site cysteine residues of AcePrx-1 Δ171 co-crystallized with conoidin A. A quinoxaline monoxide (QMO) adduct was modeled into the density and refined. The view is rotated horizontally ~90°, then vertically 180° relative to the view in panel A.

D. $2F_o$ - F_c map (blue) after refinement with the QMO adduct. See also Figure S3.

Table 1

Data collection and refinement statistics.

Data collection		
Data set name	Unliganded AcePrx-1	Δ171/conA complex
Space group	$P2_1$	$C2$
Cell dimensions		
a, *b*, *c* (Å)	64.7, 146.3, 136.0	141.6, 141.7, 68.9
β (°)	95.2	98.5
Resolution (Å)[a]	50.0-2.11 (2.15 - 2.11)	50.0-3.00 (3.11-3.00)
R_{merge}[a,b] (%)	6.3 (64.3)	7.9 (33.1)
$I / \sigma I$[a]	20.6 (2.0)	13.0 (1.8)
Completeness (%)[a]	99.7 (95.5)	74.2 (15.0)[f]
Redundancy[a]	4.0 (3.6)	3.6 (1.4)
Refinement and model quality		
Resolution range (Å)	50.0-2.11	50.0-3.00
No. reflections (working set)	129,561	18,894
No. reflections (test set)	7,228	994
R_{work} / R_{free}[c]	19.5 / 21.4	18.6 / 20.0
No. atoms		
Protein	13,404	6761
Water	605	15
Ligand	0	27
Average *B*-factors (residual after TLS refinement[d])		
Protein (Å^2)	29.7	89.6
Water (Å^2)	29.6	94.6
Ligand (Å^2)	N/A	90.0
RMS[e] deviations from ideal values		
Bond lengths (Å)	0.005	0.005
Bond angles (°)	0.95	0.96
Ramachandran plot	97.8	97.5
Favored regions (%)	2.2	2.5
Outliers (%)	0.0	0.0

[a] Highest resolution shell is shown in parentheses

[b] $R_{merge} = \Sigma_{hkl}\Sigma_i |I_{hkl,i} - \langle I \rangle_{hkl}| / \Sigma_{hkl}\Sigma_i |I_{hkl,i}|$, where I_{hkl} is the intensity of a reflection and $\langle I \rangle_{hkl}$ is the average of all observations of the reflection

[c] R_{free}, R_{work} with 5% of F_{obs} sequestered before refinement

[d] See PDB entries for TLS refinement parameters

[e] RMS, root mean square

[f]The data was >96% complete in each resolution shell up to 3.5 Å.